Absolute frequency measurement of the ^{88}Sr$^+$ clock transition using a GPS link to the SI second

View the article online for updates and enhancements.

Absolute frequency measurement of the ^{88}Sr$^+$ clock transition using a GPS link to the SI second

Pierre Dubé, John E Bernard and Marina Gertsvolf

National Research Council Canada, Ottawa, Ontario, K1A 0R6, Canada

E-mail: pierre.dube@nrc-cnrc.gc.ca

CrossMark

Abstract

We report the results of a recent measurement of the absolute frequency of the $5s\ ^2S_{1/2}$ $-4d\ ^2D_{5/2}$ transition of the ^{88}Sr$^+$ ion. The optical frequency was measured against the international atomic time realization of the SI second on the geoid as obtained by frequency transfer using a global positioning system link and the precise point positioning technique. The measurement campaign yielded more than 100 h of frequency data. It was performed with improvements to the stability and accuracy of the single-ion clock compared to the last measurement made in 2012. The single ion clock uncertainty is evaluated at 1.5×10^{-17} when contributions from acousto-optic modulator frequency chirps and servo errors are taken into account. The stability of the ion clock is 3×10^{-15} at 1 s averaging, a factor of three better than in the previous measurement. The results from the two measurement campaigns are in good agreement. The uncertainty of the measurement, primarily from the link to the SI second, is 0.75 Hz (1.7×10^{-15}). The frequency measured for the S–D clock transition of ^{88}Sr$^+$ is $\nu_0 =$ 444 779 044 095 485.27(75) Hz.

(Some figures may appear in colour only in the online journal)

1. Introduction

Several optical atomic clocks have demonstrated inaccuracies and instabilities that are significantly lower than those obtained with the best caesium (Cs) fountain clocks that realize the SI second. These benefits can be largely attributed to two factors. The first is an increase in the reference transition frequency by a factor of approximately 10^5 compared to that of the Cs microwave primary frequency standard. The second is the use of trapped and laser-cooled quantum references: ions in rf traps and neutral atoms in optical lattices. The resulting confinement to a small volume in space suppresses motion-related shifts and broadening, prevents motion through the apparatus where the electric and magnetic fields may be difficult to characterize, and allows for the long interaction times required to achieve hertz-level resolutions at optical frequencies.

Considering their exceptional performances, optical atomic clocks have become compelling candidates for a redefinition of the unit of time [1–3]. Toward this goal, it is essential to make accurate measurements of the optical frequencies relative to the current definition of the SI second and to demonstrate agreement with other laboratories. As a side benefit, high-accuracy absolute frequency measurements are used to refine the determination of the optical frequencies used as secondary representations of the second. Further tests of the accuracy and reproducibility of optical clocks, beyond the capability of the microwave standards, are obtained by performing direct optical to optical comparisons to determine frequency ratios [4]. Such comparisons are also used to investigate possible time variations in the fundamental constants [5–8].

The optical atomic clock studied at the National Research Council of Canada (NRC) is based on the $5s\ ^2S_{1/2} - 4d\ ^2D_{5/2}$ reference transition of a trapped and laser-cooled single ion

of ^{88}Sr$^+$. This ion system has also been in development for several years at the National Physical Laboratory (NPL) in the United Kingdom [9, 10]. More recently other groups are contributing to the study of the ^{88}Sr$^+$ ion for the development of optical clocks [11–13]. The 445 THz (674 nm) transition is a CIPM recommended secondary representation of the SI second [14].

In this paper, we report a recent measurement of the absolute frequency of the *S–D* reference transition of ^{88}Sr$^+$. The measurement was made relative to the SI second realized using a satellite link to international atomic time (TAI). Section 2 gives an overview of the ^{88}Sr$^+$ ion clock, with a discussion of recent advances that improve the accuracy of the unperturbed clock transition frequency. Section 3 describes the lock of the probe laser frequency to the *S–D* line center. The servo tracking uncertainties have been reduced by two-orders of magnitude compared to our previous measurement reported in 2012 [15, 16]. The uncertainty budget of the ^{88}Sr$^+$ ion clock transition frequency is presented in section 4.

The femto-second laser frequency comb system used to measure the 445 THz optical frequency is discussed in section 5. A brief description of the global positioning system (GPS) frequency link to TAI and the analysis of the raw global navigation satellite system (GNSS) data that was performed using the precise point positioning (PPP) method is given in section 6. This analysis provided the calibration of the hydrogen maser used as reference for the operation of the femto-comb laser.

The frequency measurements are reported in section 7. The final result is compared with previous measurements made at NRC and NPL in section 8. Potential avenues for future improvements in the determination of the absolute frequency of the ^{88}Sr$^+$ clock transition in our laboratory are also mentioned.

2. ^{88}Sr$^+$ ion optical frequency standard

The ^{88}Sr$^+$ optical frequency standard developed at the NRC has been described in detail previously [15–17]. Below we give a brief review with emphasis on recent advances.

A single ion of ^{88}Sr$^+$ is confined at the center of a miniature rf quadrupole trap of the end-cap design [18]. Its kinetic temperature is cooled to 2.0(5) mK using a frequency-stabilized diode laser at 422 nm, red-detuned by approximately a half-linewidth from the strongly-allowed $5s\ ^2S_{1/2} - 5p\ ^2P_{1/2}$ transition line center [11]. Decay of the $^2P_{1/2}$ state to the $^2D_{3/2}$ metastable state is prevented with a repumper laser at 1092 nm.

The optical reference is the $5s\ ^2S_{1/2} - 4d\ ^2D_{5/2}$ electric quadrupole allowed transition at 674 nm which has a natural linewidth of 0.4 Hz. It is probed using a laser source locked to an ultra-stable Fabry-Perot ULE cavity. The stabilized laser linewidth is approximately 4 Hz as determined by high-resolution spectroscopy on a single Zeeman component of the *S–D* transition [16, 19]. The state of the ion following each probe laser pulse is detected with the electron shelving method, by monitoring the 422 nm fluorescence with a photo-multiplier tube.

The ion trap is housed in an ultra-high vacuum chamber and shielded from ambient magnetic fields with two concentric mu-metal magnetic shields. Three pairs of Helmholtz coils mounted on the optical access ports of the vacuum chamber provide precise control of the magnetic field vector at the ion. For the experiments reported here, a small magnetic field of $\approx$0.6 μT was aligned along the vertical direction, parallel to the 422 nm cooling laser beam for state-preparation. The magnetic field was also used to split the *S–D* transition into ten Zeeman components distributed as five symmetric pairs about line center. The probe laser beam direction was perpendicular to magnetic field, with the consequence that the innermost ($\Delta m_J = 0$) components of the Zeeman spectrum had vanishing intensities. The average of the line centers of any symmetric pair gives the virtual line center of the clock transition with the linear Zeeman shift removed. A very significant improvement in the accuracy of the ion clock frequency is obtained by extending the method to include three pairs of Zeeman components that connect to the six magnetic sublevels of the $^2D_{5/2}$ state of the clock transition. Since the innermost components could not be used, the second, third and fourth pairs were selected to connect to all of the $^2D_{5/2}$ sublevels. The average over the sublevels has the property that it rigorously cancels the electric quadrupole shift and the tensor Stark shifts [16, 20].

An exception in our experiments was the ac tensor Stark shift caused by the 674 nm light. It was not strongly suppressed because the laser power was adjusted for each symmetric pair of components as described below. This limitation has a negligible impact on the error budget because the shift is estimated to be below the 10^{-20} level even when there is no cancellation from Zeeman averaging [16, 21].

In our experiments, averaging over the magnetic sublevels energies of the $^2D_{5/2}$ state is implemented by independently locking the probe laser frequency to six resonances from three symmetric pairs of Zeeman components. The line center of each resonance is predicted based on its previously measured value, the current drift rate of the reference ULE cavity, and the elapsed time since the last measurement. The laser frequency is then tuned using a double-pass acousto-optic modulator (AOM) a half-linewidth below and a half-linewidth above the predicted line center for measurement of the excitation probabilities on each side of the resonance. The offset of the laser frequency from line center is evaluated from the excitation probability imbalance and knowledge of the resonance lineshape [22]. The measurement is repeated for the other resonances, and cycles continuously through the sequence. The frequencies are continuously averaged to determine the unperturbed *S–D* line center.

For optimum stability, the ion is state-prepared before each probe laser pulse. State preparation is performed during the second half of the cooling pulse; the first half is reserved for state detection. As soon as state detection is completed, a pulse of laser radiation at 1033 nm transfers the ion from the $^2D_{5/2}$ state to the short-lived $^2P_{3/2}$ state from where the ion decays to the ground state in a few ns. The polarization of the 422 nm laser radiation is switched to circular (σ^+ or σ^-) for $\approx$2 ms at the end of the cooling pulse for optical pumping into the
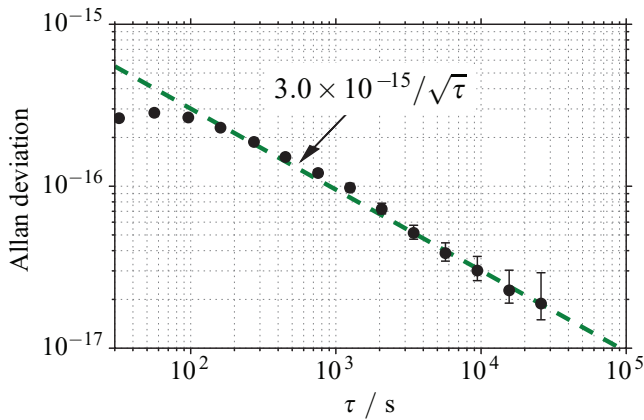
Figure 1. Overlapping Allan deviation as a function of averaging time of the probe laser frequency corrections during a lock run to the ion line center. The data are reported as solid circles with error bars estimated by assuming white frequency noise. The dashed line is a fit to the data with a slope of $-1/2$ and an intercept of 3×10^{-15} at 1 s averaging. The data are from a lock that lasted 115 000 s. The probe laser pulses were 100 ms long. The Allan deviation was estimated by treating the locks to each symmetric pair as independent, thus providing three 'clocks' that were intercompared to determine the Allan deviation. The results were averaged and corrected to give the stability of the laser locked to the *S–D* line center [17].

ground-state magnetic sublevel of interest. State preparation ensures that the ion is in the lower magnetic sublevel of the probed transition with a probability of 99% or better. The probe laser power is also adjusted for on-resonance π-pulse excitation to maximize the transition probabilities. A different laser power, controlled with the double-pass AOM, is usually required for each symmetric pair of components. The instability achieved for the lock of the probe laser frequency to the ion line center is $\approx 3 \times 10^{-15}$ at 1 s averaging, a level that approaches the quantum projection noise limit for a single ion of ^{88}Sr$^+$ [17].

Figure 1 gives an example of the stability observed. The data were recorded with 100 ms probe laser pulses and a dead time of 29 ms for cooling and state preparation. The Fourier transform limited Rabi lineshape had a linewidth of 8 Hz with an excitation probability on resonance of approximately 85%, primarily determined by the lifetime of the $^2D_{5/2}$ state and the ion kinetic temperature. The interrogation rate of the clock transition was 7.7 Hz and the cycle time through the six resonances was 48 s. These lock parameters were typical settings for the frequency measurements reported in this paper.

The ion trap was driven at a frequency of $\Omega_0/2\pi = 14.408$ MHz with a voltage amplitude of 212 V between endcap and shield electrodes. The observed secular frequencies were $\nu_x \simeq 1132$ MHz, $\nu_y \simeq 1150$ MHz, and $\nu_z \simeq 2247$ MHz. At the special drive frequency Ω_0 mentioned above, the micromotion-induced second-order Doppler shift and the scalar Stark shift cancel each other. This is possible for the *S–D* transition of ^{88}Sr$^+$ because its differential static scalar polarizability, $\Delta\alpha_0$, is negative [23]. For our system, the level of suppression is at least 215 when compared to either micromotion shift taken separately. The suppression level is limited by the difference between the restoring forces in the axial and radial

directions (Mathieu parameters q_r and q_z) rather than by the uncertainty of $\Delta\alpha_0$; the optimum Ω_0 is slightly different for motion along the axial direction than it is for motion along the radial direction [23, 24].

The micromotion shifts were also minimized by adjusting the voltages of trim electrodes while monitoring the effect of changing the trap depth on the ion position with a camera. A quantitative evaluation of the micromotion levels was obtained by measuring the sideband-to-carrier intensity ratio of a Zeeman component for three mutually orthogonal directions of the probe laser beam [16]. A study of micromotion following minimization with the camera gave a contribution of $3(1) \times 10^{-17}$ for either micromotion shift. Taking into account the suppression at a trap drive frequency of Ω_0, the net micromotion shift is reduced to zero with a fractional uncertainty of 10^{-19}.

3. ^{88}Sr$^+$ servo tracking errors

The largest uncertainty associated with the ^{88}Sr$^+$ ion clock during the measurement of 2012 was caused by servo tracking errors of 0.12(3) Hz or $2.7(7) \times 10^{-16}$ in fractional units [16]. Although this level of uncertainty is well below the uncertainty of the absolute frequency measurement of 2×10^{-15}, it required data post-processing for evaluation. It also degraded significantly the ultimate accuracy of the clock, evaluated at 2×10^{-17} at the time. The main causes for the tracking errors were the use of a constant cavity drift rate in the servo algorithm, an approximate method of setting the servo gain, and a long cycle time of ≈ 200 s through the six resonances.

The servo algorithm used for the measurements reported here was modified to include a continuous evaluation of the cavity drift rate based on an exponentially weighted moving average of previously determined rates. The algorithm takes the following form:

$$D_n = [\, d_n + (N-1)D_{n-1} \,]/N, \tag{1}$$

where D_n is the exponential moving average of the cavity drift rate for measurement n and D_{n-1} that for the previous measurement. $d_n = (f_n - f_{n-6})/\Delta T$ is the drift rate determined from the two most recent measurements of a given Zeeman component line center, f_n and f_{n-6}. The two frequencies are separated by six steps, corresponding to the number of different Zeeman components interrogated during a complete cycle. ΔT is the time between measurements, equal to the cycle time through the six components. Every time a component line center is measured, the average drift rate is updated. The averaging is controlled by the parameter N. We used a value of $N = 150$ for the experiments reported here. For an alternative implementation of cavity drift rate compensation see, for example, [25].

Figure 2(a) gives an example of the cavity drift rate measured during the lock using the exponential moving average. Also shown is the drift rate evaluated in post processing to obtain reference data without a time lag. Figure 2(b) shows the residuals between these two evaluations. The slower fluctuations are caused by a ≈ 20 min lag in the drift rates evaluated
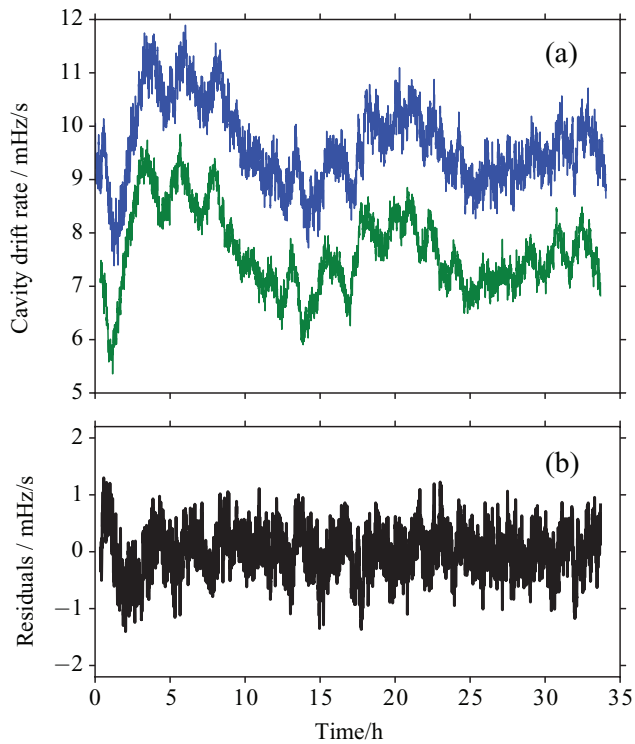
Figure 2. (a) Reference cavity drift rate as a function of time. The top curve shows the rate determined using an exponential moving average. It was used to predict the line center positions of the *S–D* Zeeman components. For comparison, the lower curve shows the cavity drift rate evaluated in post-processing with a deliberate offset of -2 mHz s^{-1} to separate the curves. (b) Residuals obtained by taking the difference between the two curves in (a). The fast fluctuations are caused by measurement noise and the slower ones by a lag in the exponential moving average compared to the post-processed data.

using the exponential moving average. The drift rate errors fluctuate about zero, with excursions typically within ± 1 mHz s^{-1}. Short term biases usually average to insignificant levels after a few hours of measurement because the changes in drift rates are as much positive as they are negative in long lock runs. The isothermal creep of the reference ULE cavity has not deviated much from 10 mHz s^{-1} for several years and changes in drift rates usually reverse sign after a few hours or less [19].

The implementation of state-preparation discussed in section 2 resulted in an increase in the quantum jump rate and allowed a decrease in the cycle time from 200 s in the measurements reported in 2012 [15, 16] to 48 s. The shorter cycle time contributes to a direct reduction in the servo tracking errors by a factor of approximately four.

There is an optimum gain that can eliminate servo tracking errors [16, 17]. This optimum, however, requires an accurate knowledge of the resonance lineshape which depends on the probe laser pulse duration, the pulse excitation area, and the laser linewidth. For the experiments reported here, the Rabi lineshape was calculated for the ideal case of π-pulse excitation and Fourier transform limited linewidths [17]. These assumptions are reasonable but not exact. Allowing for 10% variations in pulse area and resonance linewidth, the servo errors are estimated to be at the mHz level or lower ($\lesssim 2 \times 10^{-18}$) for the present series of measurements.

Table 1. Leading fractional frequency shifts ($\Delta\nu/\nu_0$) and uncertainties (σ/ν_0) of the $^2S_{1/2}$–$^2D_{5/2}$ transition of ^{88}Sr$^+$, including measurement effects. ν_0 is the 445 THz *S–D* frequency.

Source of shift	$\frac{\Delta\nu}{\nu_0}/10^{-18}$	$\frac{\sigma}{\nu_0}/10^{-18}$
BBR field evaluation, $\langle E^2 \rangle_T$	557	11
AOM chirps	0	10
1092 nm ac Stark shift	-4	2
Collisional shift	0	2
Servo tracking errors	0	2
BBR coefficient, $\Delta\alpha_0$	0	0.83
Thermal motion	-3.2	0.8
Excess micromotion	0	0.1
Electric quadrupole shift	0	0.03
Total	550	15

4. ^{88}Sr$^+$ uncertainty budget

Table 1 summarizes the leading systematic shifts and uncertainties of the ^{88}Sr$^+$ ion clock for the measurements reported in this work. A detailed discussion of the uncertainty budget that includes smaller effects can be found in [16]. In table 1, the evaluated uncertainties of the 1092 nm ac Stark shift and collisional shift are identical to those of the earlier work. The second-order Doppler and Stark shifts caused by thermal motion in the pseudo-potential were re-evaluated for an ion kinetic temperature of 2.0(5) mK. The dominant contributions are from the second-order Doppler shifts at the secular frequencies. The micromotion shifts associated with thermal motion are strongly suppressed because their frequency components are close to the special rf trap drive frequency Ω_0 chosen for optimal suppression of the second-order Doppler and scalar Stark shifts. Operation of the trap at the frequency Ω_0 reduces the thermal motion shifts by a factor of almost three compared to an identical system with a positive $\Delta\alpha_0$ parameter. The servo tracking errors were presented in section 3. The other frequency shifts are discussed below.

The black body radiation (BBR) shift, $\Delta\nu_{\text{BBR}}$, in hertz, is given by [26, 27]

$$\Delta\nu_{\text{BBR}} = -\frac{1}{2h}\langle E^2 \rangle_T \, \Delta\alpha_0(1+\eta), \qquad (2)$$

where h is Planck's constant, $\langle E^2 \rangle_T$ is the mean squared electric field at the ion caused by thermal radiation, $\Delta\alpha_0$ is the differential static scalar polarizability of the *S–D* transition introduced in section 2, and η is the dynamic correction.

The atomic parameter $\Delta\alpha_0$ was evaluated with high accuracy recently, with a reduction of its contribution to the uncertainty budget from 2×10^{-17} to 8.3×10^{-19} [23]. η is known from atomic structure calculations with an accuracy of 8.4×10^{-20} [23, 28]. The evaluation of $\langle E^2 \rangle_T$ yields the largest uncertainty contribution of 1.1×10^{-17} in our system. Its evaluation is the same as previously reported [16], but corrected for the average vacuum chamber temperature of 22.8(2) °C observed during the measurements reported here.

As discussed in section 2, the minimized micromotion shifts are reduced by a factor of 215, to a level of 10^{-19}, by using an rf trap drive frequency determined by the atomic parameter $\Delta\alpha_0$. This effect was also used in the previous

measurements, but $\Delta\alpha_0$ was known with less accuracy which limited the suppression to a factor estimated at 28 at the time.

The electric quadrupole shift (EQS) should, in principle, vanish with averaging of the $^2D_{5/2}$ magnetic sublevel energies. During a lock to the ion line center, however, measurement of the resonances is sequential and it is possible that drifts in the EQS cause a shift because the resonances are not measured simultaneously. The uncertainty of the cancellation is estimated to be $\lesssim 3 \times 10^{-20}$ using a simulation based on lock data [16]. The new evaluation is at least an order of magnitude lower than in 2012 for two main reasons. The first is that a higher transition probability was obtained with state preparation, allowing a reduction of the cycle time by a factor of four as mentioned earlier. The second is a reduction of the EQS magnitude by a factor of 6(2) that has resulted from a change in the quantization axis direction for state preparation. The effect stems from the $(3\cos^2\theta - 1)$ dependence of the EQS on the angle θ between the electric field gradient and the quantization axis. For a magnetic field along the vertical direction, as used in the current study, we measured $\theta = 53(2)°$, close to the ideal value of $\theta = \cos^{-1}(1/\sqrt{3}) = 54.7°$ where the $(3\cos^2\theta - 1)$ factor reduces to zero. Previously, the residual background magnetic field was used as the quantization axis and the angle of $\theta = 44(2)°$ was less favorable for reduction of the EQS.

The 674 nm probe laser pulses were created by modulating the drive power of the double-pass AOM that was also used to control the optical frequency. Modulation of the rf power causes temperature variations in the TeO_2 crystal of the AOM that can result in frequency shifts [6, 29]. We have investigated this effect experimentally using a heterodyne Mach-Zehnder interferometer, to compare the double-pass AOM path length changes to a reference beam sampled before the AOM. For 100 ms rf pulses separated by 29 ms, the maximum AOM drive power of 1.3 W produced shifts of approximately 15 mHz. They were found to scale linearly with drive power as observed in other studies [6, 29]. Correcting for the rf powers used in the experiments, the maximum shift is estimated to be below 5 mHz (1×10^{-17}). This maximum value is taken as the uncertainty of the AOM frequency chirps in table 1. Although its contribution is comparable to that of the thermal BBR field in the present study, it can easily be reduced to insignificant levels by reducing the rf drive power by 15 dB or more.

The total shift and uncertainty of the ion frequency reported in table 1 is $55.0(1.5) \times 10^{-17}$ in fractional units, which corresponds to 0.245(7) Hz at 445 THz.

5. Femto-second laser frequency comb

A fiber-based femto-second laser frequency comb, referenced to a hydrogen maser, was used for the absolute frequency measurement of the 674 nm laser [30]. Since the fiber comb operates at infrared wavelengths of $\approx 1–2\ \mu$m, a portion of the comb near 1348 nm was frequency doubled to 674 nm in periodically poled MgO:LiNbO$_3$ (PPLN). An optical fiber with

active fiber noise cancellation was used to bring the 674 nm probe laser light to the frequency comb laboratory where it was combined with the doubled comb light on an avalanche photodiode. An rf tracking oscillator was locked to the resulting beat signal, f_B, that had a signal-to-noise ratio (S/N) of ≈ 30 dB in a 100 kHz measurement bandwidth. The frequency of the rf tracking oscillator was counted using a zero-deadtime counter (Pendulum CNT-91). Previous measurements showed that while f_B could be counted directly, the use of the tracking oscillator permitted reliable counting over longer periods of unattended operation. The accuracy of the counter was investigated by comparing it to another zero-deadtime counter (Keysight 53230A) in a series of test measurements of the probe laser frequency. Both counters used a gate period of 1 second, but the gates were not synchronized. The agreement between the counters was typically better than 10 mHz after a few hours of measurement. These counters were in agreement within the uncertainty determined by the Allan deviation.

A second tracking oscillator was used as part of the comb's f-to-2f phase-lock. This tracking oscillator was phase-locked to the carrier-envelope offset frequency, f_{ceo}, with an offset of 20 MHz and permitted long-term, unattended operation of the comb. The frequency of the tracking oscillator was counted during the measurements to check for cycle slips in the f-to-2f phase-lock. The 20 MHz offset frequency was also counted in order to detect any cycle slips in the lock of the tracking oscillator to f_{ceo}. These cycle slips which were clearly evident by counter readings which differed from 20 MHz by integer values, occurred at a rate of approximately one every thousand seconds and were accounted for in the analysis of the comb data. Similar measurements of the 20 MHz offset frequency in the lock of the first tracking oscillator to the f_B signal showed no evidence of cycle slips for the S/N levels used in the measurements.

6. GPS link to the SI second

At NRC we achieve traceability to the SI second via GNSS time and frequency transfer and Circular-T reports. Typically the satellite navigation system data from the NRC3 (Ashtech) receiver is submitted to the Bureau International des Poids et Mesures (BIPM) where it is processed using the BIPM implementation [31] of the PPP software [32]. During the measurement campaign reported here, the performance of NRC3 had degraded and its data could not be used for the PPP calculations. Instead, we used satellite observation data from other GPS receivers at NRC and our own implementation of the PPP software from NRCan, CSRS–PPP [33].

We first validated the NRC PPP implementation by comparing the NRC results with those published by BIPM for several international laboratories: the National Physical Laboratory (NPL), the Physikalisch-Technische Bundesanstalt (PTB), the Observatoire de Paris (OP), and the United States Naval Observatory (USNO). We generated PPP output for the data from each laboratory for a period of thirty days, similar to that of BIPM publications, and computed the differences between pairs of laboratories. This way

Table 2. Comparison of NRC and BIPM analysis of RINEX data from a few laboratories for the month of December 2015. Values represent the average offset between the laboratories and are expressed in fractional frequency units of 1×10^{-15}. The right column shows the difference between NRC and BIPM results.

	NRC	BIPM	NRC-BIPM
USNO-NPL	2.0	2.3	-0.3
USNO-PTB	0.2	0.0	0.2
USNO-OP	-0.5	-0.4	-0.1

Table 3. Comparison of several NRC and USNO receivers for the month of February 2016. Values represent the difference between NRCi and USNi and are expressed in fractional frequency units of 1×10^{-15}. The top row identifies the antenna used with the receivers.

	Novatel		Ashtech	
	NRC2	NRC7	NRC4	NRC8
USN6	-3.3	-3.3	-4.2	-3.8
USN7	-3.2	-3.2	-4.1	-3.7

Table 4. Estimated fractional frequency uncertainty of the GPS link to the SI second.

Source of uncertainty	Unc. / 10^{-15}
NRC–USNO	1.0
Variation between receivers and antennas	0.9
USNO–TAI	0.5
TAI–TT	0.3
PPP implementation	0.3
Total	1.5

Table 5. Uncertainty budget for the absolute frequency measurement of the ^{88}Sr$^+$ ion S–D transition.

Source of shift	Shift / Hz	Unc. / Hz
GPS link to the SI second	[a]	0.67
Measurement statistics	0	0.34
^{88}Sr$^+$ ion clock	0.245	0.007
Gravitational redshift	4.648	0.001
Total	4.893	0.75

[a] Included separately.

the reference timescales and the configuration differences between the two PPP methods cancel out. From the results shown in table 2 we find that the resulting frequency variation between the two implementations is less than 0.3×10^{-15}. We use this value as the uncertainty estimate of our PPP software implementation.

Next, we investigated the reproducibility of GPS frequency transfer by comparing the results obtained with various antennas and receivers. PPP calculations were performed for the NRC2 (Javad), NRC4 (Septentrio), NRC7 (Novatel) and NRC8 (Topcon) receivers that NRC operates, and compared against two USNO receivers, USN6 and USN7. All NRC receivers used a time base signal derived from a common hydrogen maser. NRC2 and NRC7 are connected to a Novatel antenna, while NRC3, NRC4 and NRC8 are connected to an Ashtech antenna. Both antennas are located on the roof of the building and have a clear view of the sky. The results, summarized in table 3, show that the maximum variation observed when using different hardware was 0.9×10^{-15}. This value is taken as the uncertainty introduced by the antennas and the receivers.

The NRC clock used for the UTC(NRC) realization and, therefore, traceability to the SI second, is a commercial Cs standard that does not have the stability and accuracy required to achieve a frequency uncertainty at the 10^{-15} level. We rely instead on the stability of the USNO timescale for a link to the SI second and the PPP calculations. The uncertainty of the frequency offset between NRC and USNO is estimated to be 1×10^{-15} derived from the Allan deviation of the PPP frequency transfer between NRC and USNO.

The complete link also requires knowledge of the offset between USNO and TAI, and between TAI and the SI second. These quantities and their uncertainties were obtained from the analysis of the data from circular-T reports published monthly by BIPM. The uncertainty budget of the link to the SI second for the measurements reported here is summarized

in table 4. The total standard uncertainty of the GPS link is estimated to be 1.5×10^{-15} in fractional units, or 0.67 Hz at the ion clock transition frequency of 445 THz.

7. Absolute frequency measurement

The determination of the ion frequency with respect to the SI second was achieved by combining three sets of data recorded simultaneously. The first set is the lock of the probe laser frequency to the ion line center. The second set is obtained with the frequency comb that measures the probe laser frequency with respect to the reference hydrogen maser, and the last one is the calibration of the maser using a GPS link to the SI second.

The uncertainty budget and frequency shifts of the ^{88}Sr$^+$ ion frequency measurement are summarized in table 5. The GPS frequency transfer uncertainty was discussed in section 6, and the uncertainty and shift of the ^{88}Sr$^+$ clock transition frequency in section 4. The measured frequencies must also be corrected for the gravitational redshift at the ion's location. To that end, the height of the ion clock above the geoid was measured accurately [34] and recently updated using the latest geoid height model for Canada called the Canadian geodetic vertical datum of 2013 (CGVD 2013) [35]. Taking into account the 3.2 mm/year vertical speed of the building and the time elapsed since the height was determined, we find an ion clock height of 95.778(24) m. Knowing that the local gravitational acceleration is 9.8062 m s^{-2}, we find a gravitational redshift at 445 THz of 4.648(1) Hz.

The frequency measurements, corrected for the total shift of 4.893 Hz and the hydrogen maser calibration, are shown in figure 3. The measurement campaign spanned more than two months, with most of the measurements taken over a two-week period. The total measurement time was 103 h. The error bars shown in figure 3(a) were evaluated based on the Allan deviation of each uninterrupted comb measurement of the probe laser frequency.
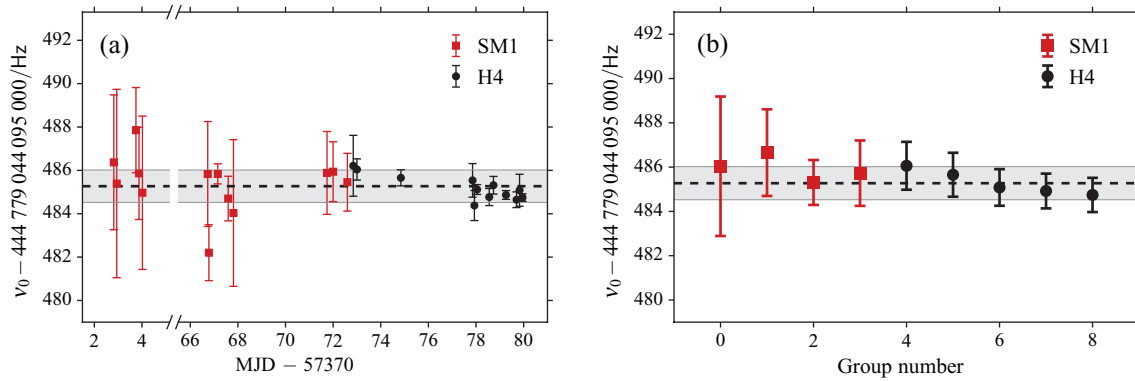
Figure 3. (a) Measurements of the *S–D* clock transition frequency of the ^{88}Sr$^+$ ion, ν_0, versus the modified Julian date (MJD). The frequencies were corrected for the known frequency shifts. Two different masers were used as reference for the femto-second laser frequency comb during the measurements. The filled squares were obtained using a Symmetricom MHM 2010 (SM1), while the filled circles indicate measurements made with an NRC-built hydrogen maser (H4). (b) Weighted means of the measurements in (a) grouped into bins of approximately 1 day (see text). The ion frequency, determined from the weighted mean of the grouped data, is 444 779 044 095 485.27 Hz. It is shown by a horizontal dashed line in each subfigure. The total standard uncertainty of 0.75 Hz ($k = 1$) is also indicated in each subfigure by a shaded area delimited by solid gray lines.
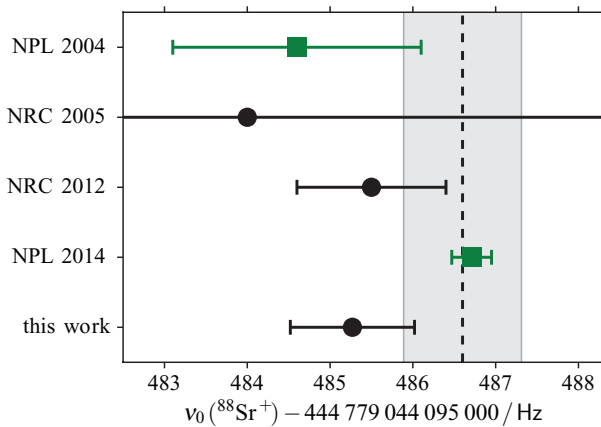

Figure 4. Comparison of absolute frequency measurements of the *S–D* transition of ^{88}Sr$^+$. Laboratory identification and year of publication are given on the *y*-axis. The references are NPL 2004 [9], NRC 2005 [20], NRC 2012 [15], and NPL 2014 [10]. The 15 Hz standard uncertainty of the NRC 2005 measurement is outside the bounds of the figure. The filled squares indicate measurements made with a Cs fountain clock as reference and the filled circles with a GPS link to the SI second. The 2015 CIPM recommended frequency is shown as the vertical dashed line and its assigned uncertainty by the shaded area [14].

The data were grouped into bins of approximately 1 day to avoid giving disproportionate weight to measurements that have very low statistical uncertainties. The values displayed in figure 3(b) are the weighted means of the binned data. We took the sample standard deviation of the binned data of 0.62 Hz as representative of the statistical uncertainty for one day of measurement. This uncertainty was added in quadrature with that of the binned data, and the result was used as the uncertainty of each point in figure 3(b). The ion frequency was determined from the weighted mean of the binned data. The overall statistical uncertainty of the frequency measurement is 0.34 Hz and the total evaluated standard uncertainty is 0.75 Hz (1.7×10^{-15}) as reported in table 5. After accounting for all

shifts and their uncertainties, the unperturbed ion frequency obtained is 444 779 044 095 485.27(75) Hz.

8. Comparison with earlier measurements

Figure 4 summarizes the absolute frequency measurements of the 445 THz transition of ^{88}Sr$^+$ made since 2004. The 2015 CIPM recommended value is also shown with its uncertainty for comparison. It is based on the weighted mean of the previously published results shown in figure 4. The CIPM value is strongly biased towards a recent measurement that has an evaluated uncertainty of 0.24 Hz [10]. The agreement between the measurements is generally consistent with the uncertainties. If we restrict the comparison to our laboratory, the agreement is much better, indicating good reproducibility of the GPS frequency transfer and ion clock operation despite several changes made over the years.

9. Conclusion

We have reported a new measurement of the $5s\ ^2S_{1/2} - 4d\ ^2D_{5/2}$ transition of the ^{88}Sr$^+$ ion made with a GPS link to the SI second. Compared to a previous measurement reported in 2012, the operation and accuracy of the ^{88}Sr$^+$ ion clock have been improved. For example, the servo tracking errors were reduced to 2×10^{-18} and the accuracy of the ion clock has been improved with a recent determination of the differential static scalar polarizability of the clock transition. Better knowledge of this atomic parameter has reduced the uncertainty of the BBR shift evaluation and has allowed a strong suppression of the micromotion shifts. The overall fractional uncertainty of the ^{88}Sr$^+$ clock during the measurement campaign was 1.5×10^{-17}.

The *S–D* ion frequency was measured with a fractional uncertainty of 1.7×10^{-15}, limited mainly by the GPS link analyzed using the PPP method and by the statistical uncertainty

of the measurements. Comparison of the new value with previous results from NRC and NPL shows reasonable agreement, consistent with the evaluated uncertainties.

Recent developments in GPS data analysis using the PPP method with integer ambiguity resolution (IPPP) are expected to improve significantly on the potential accuracy of the satellite link and to open promising perspectives for remote comparison of microwave and optical clocks at the 1×10^{-16} level [36, 37]. Furthermore, a Cs fountain clock is expected to become available at NRC in the near future for direct absolute frequency measurements at the low 10^{-16} level [38]. These advances are expected to yield a determination of the *S–D* frequency of $^{88}Sr^+$ in our laboratory that approaches the current accuracy limit of primary frequency standards.

References

[1] Gill P 2011 When should we change the definition of the second? *Phil. Trans. R. Soc.* A **369** 4109–30

[2] Riehle F 2012 Optical atomic clocks could redefine unit of time *Physics* **5** 126

[3] Gill P 2016 Is the time right for a redefinition of the second by optical atomic clocks? *J. Phys.: Conf. Ser.* **723** 012053

[4] Margolis H S and Gill P 2015 Least-squares analysis of clock frequency comparison data to deduce optimized frequency and frequency ratio values *Metrologia* **52** 628

[5] Fortier T M *et al* 2007 Precision atomic spectroscopy for improved limits on variation of the fine structure constant and local position invariance *Phys. Rev. Lett.* **98** 070801

[6] Rosenband T *et al* 2008 Frequency ratio of Al$^+$ and Hg$^+$ single-ion optical clocks; metrology at the 17th decimal place *Science* **319** 1808–12

[7] Godun R M, Nisbet-Jones P B R, Jones J M, King S A, Johnson L A M, Margolis H S, Szymaniec K, Lea S N, Bongs K and Gill P 2014 Frequency ratio of two optical clock transitions in $^{171}Yb^+$ and constraints on the time variation of fundamental constants *Phys. Rev. Lett.* **113** 210801

[8] Huntemann N, Lipphardt B, Tamm C, Gerginov V, Weyers S and Peik E 2014 Improved limit on a temporal variation of m_p/m_e from comparisons of Yb$^+$ and Cs atomic clocks *Phys. Rev. Lett.* **113** 210802

[9] Margolis H S, Barwood G P, Huang G, Klein H A, Lea S N, Szymaniec K and Gill P 2004 Hertz-level measurement of the optical clock frequency in a single $^{88}Sr^+$ ion *Science* **306** 1355–8

[10] Barwood G P, Huang G, Klein H A, Johnson L A M, King S A, Margolis H S, Szymaniec K and Gill P 2014 Agreement between two $^{88}Sr^+$ optical clocks to 4 parts in 10^{17} *Phys. Rev.* A **89** 050501

[11] Lindvall T, Merimaa M, Tittonen I and Madej A A 2012 Dark-state suppression and optimization of laser cooling

and fluorescence in a trapped alkaline-earth-metal single ion *Phys. Rev.* A **86** 033403

[12] Fordell T, Lindvall T, Dubé P, Madej A A, Wallin A E and Merimaa M 2015 Broadband, unpolarized repumping and clearout light sources for Sr$^+$ single-ion clocks *Opt. Lett.* **40** 1822–5

[13] Shaniv R, Akerman N and Ozeri R 2016 Atomic quadrupole moment measurement using dynamic decoupling *Phys. Rev. Lett.* **116** 140801

[14] Recommendation 2 (CI-2015) 2015 *Session II of the 104th Meeting of the CIPM* (www.bipm.org/utils/en/pdf/CIPM/CIPM2015-II-EN.pdf)

[15] Madej A A, Dubé P, Zhou Z, Bernard J E and Gertsvolf M 2012 $^{88}Sr^+$ 445 THz single-ion reference at the 10^{-17} level via control and cancellation of systematic uncertainties and its measurement against the SI second *Phys. Rev. Lett.* **109** 203002

[16] Dubé P, Madej A A, Zhou Z and Bernard J E 2013 Evaluation of systematic shifts of the $^{88}Sr^+$ single-ion optical frequency standard at the 10^{-17} level *Phys. Rev.* A **87** 023806

[17] Dubé P, Madej A A, Shiner A and Jian B 2015 $^{88}Sr^+$ single-ion optical clock with a stability approaching the quantum projection noise limit *Phys. Rev.* A **92** 042119

[18] Schrama C A, Peik E, Smith W W and Walther H 1993 Novel miniature ion traps *Opt. Commun.* **101** 32–6

[19] Dubé P, Madej A A, Bernard J E, Marmet L and Shiner A D 2009 A narrow linewidth and frequency-stable probe laser source for the $^{88}Sr^+$ single ion optical frequency standard *Appl. Phys.* B **95** 43–54

[20] Dubé P, Madej A A, Bernard J E, Marmet L, Boulanger J-S and Cundy S 2005 Electric quadrupole shift cancellation in single-ion optical frequency standards *Phys. Rev. Lett.* **95** 033001

[21] Madej A A, Bernard J E, Dubé P, Marmet L and Windeler R S 2004 Absolute frequency of the $^{88}Sr^+$ 5s $^2S_{1/2}$–4d $^2D_{5/2}$ reference transition at 445 THz and evaluation of systematic shifts *Phys. Rev.* A **70** 012507

[22] Bernard J E, Marmet L and Madej A A 1998 A laser frequency lock referenced to a single trapped ion *Opt. Commun.* **150** 170–4

[23] Dubé P, Madej A A, Tibbo M and Bernard J E 2014 High-accuracy measurement of the differential scalar polarizability of a $^{88}Sr^+$ clock using the time-dilation effect *Phys. Rev. Lett.* **112** 173002

[24] Dubé P, Madej A A, Tibbo M and Bernard J E 2014 Measurement of the static scalar polarizability of the $^{88}Sr^+$ clock transition *Proc. of the 28th European Frequency and Time Forum (Neuchâtel, Switzerland, 23–26 June 2014)* (IEEE) pp 443–6

[25] Peik E, Schneider T and Tamm C 2006 Laser frequency stabilization to a single ion *J. Phys. B: At. Mol. Opt. Phys.* **39** 145–58

[26] Itano W M, Lewis L L and Wineland D J 1982 Shift of $^2S_{1/2}$ hyperfine splittings due to blackbody radiation *Phys. Rev.* A **25** 1233–5

[27] Porsev S G and Derevianko A 2006 Multipolar theory of blackbody radiation shift of atomic energy levels and its implications for optical lattice clocks *Phys. Rev.* A **74** 020502

[28] Jiang D, Arora B, Safronova M S and Clark C W 2009 Blackbody-radiation shift in a $^{88}Sr^+$ ion optical frequency standard *J. Phys. B: At. Mol. Opt. Phys.* **42** 154020

[29] Degenhardt C, Nazarova T, Lisdat C, Stoehr H, Sterr U and Riehle F 2005 Influence of chirped excitation pulses in an optical clock with ultracold calcium atoms *IEEE Trans. Instrum. Meas.* **54** 771–5

[30] Bernard J E, Dubé P, Madej A A, Cundy S, Boulanger J-S, Jiang J and Jones D J 2010 Fiber-laser-based clockwork for long-term measurements and comparisons of visible optical frequency standards *Eur. Phys. J.* D **57** 247–52

[31] Petit G 2009 The TAIPPP pilot experiment *IEEE Int. Frequency Control Symp. Joint with the 22nd European Frequency and Time Forum* (IEEE) pp 116–9

[32] Ray J and Senior K 2005 Geodetic techniques for time and frequency comparisons using GPS phase and code measurements *Metrologia* **42** 215

[33] Mireault Y, Tétreault P, Lahaye F, Héroux P and Kouba J 2008 Online precise point positioning: a new, timely service from Natural Resources Canada *GPS World* **19** 59–64 (http://gpsworld.com/resources/archives/#2008)

[34] Silliker J and Belzile A 2011 Height difference for the strontium ion optical frequency standard at the National Research Council of Canada *Technical Report* Geodetic Survey Division, Natural Resources Canada

[35] Véronneau M and Huang J 2016 The Canadian geodetic vertical datum of 2013 *Geomatica* **70** 9–19

[36] Petit G, Kanj A, Loyer S, Delporte J, Mercier F and Perosanz F 2015 1×10^{-16} frequency transfer by GPS PPP with integer ambiguity resolution *Metrologia* **52** 301

[37] Hachisu H, Petit G and Ido T 2016 Absolute frequency measurement with uncertainty below 1×10^{-15} using international atomic time *Appl. Phys.* B **123** 34

[38] Beattie S, Alcock J, Jian B, Gertsvolf M and Bernard J 2016 Status of the atomic fountain clock at the National Research Council of Canada *J. Phys.: Conf. Ser.* **723** 012008